# Ultrafast Pump−Probe Study of Excited-State Charge-Transfer Dynamics in Umecyanin from Horseradish Root

**Ines Delfino,[†] Cristian Manzoni,[‡] Katsuko Sato,[§] Christopher Dennison,[§] Giulio Cerullo,[‡] and Salvatore Cannistraro*,[†]**

*Biophysics and Nanoscience Centre, CNISM - Università della Tuscia, Largo dell'Università, I-01100 Viterbo, Italy, ULTRAS-CNR-INFM, Dipartimento di Fisica, Politecnico di Milano, Piazza Leonardo da Vinci 32, I-20133 Milano, Italy, and Institute for Cell and Molecular Biosciences, Medical School, University of Newcastle upon Tyne, Newcastle upon Tyne, NE2 4HH, U.K.*

*Received: May 11, 2006; In Final Form: July 4, 2006*

We have applied femtosecond pump−probe spectroscopy to investigate the excited-state dynamics of umecyanin from horseradish roots, by exciting its 600-nm ligand-to-metal charge-transfer band with a 15-fs pulse and probing over a broad range in the visible region. The decay of the pump-induced ground-state bleaching is modulated by clearly visible oscillations and occurs exponentially with a time constant depending on the observed spectral component of the transmission difference signal, ranging from 270 fs up to 700 fs. The slower decaying process characterizes the spectral component corresponding to the metal-to-ligand charge-transfer transition. The excited-state decay rate is significantly lower than in other blue copper proteins, probably because of the larger energy gap between ligand- and metal-based orbitals in umecyanin. Wavelength dependence of the recovery times could be due to either the excitation of several transitions or the occurrence of intramolecular vibrational relaxation within the excited state. We also find evidence of a hot ground-state absorption, at 700 nm, persisting for several picoseconds. The vibrational coherence induced by the ultrashort pump pulse allows vibrational activity to be observed, mainly in the ground state, as expected in a system with fast excited-state decay. However, we find evidence of a rapidly damped oscillation, which we assign to the excited state. Finally, the Fourier transform of the oscillatory component of the signal presents additional bands in the low-frequency region which are assigned to collective motions of the protein.

## 1. Introduction

Umecyanin (UMC) from horseradish roots is an electron-transfer (ET) protein, belonging to the stellacyanin class of the phytocyanins.[1,2] The protein has the typical properties of a cupredoxin including an intense ligand-to-metal charge transfer (LMCT) absorption band at 606 nm (with a weaker LMCT band at ∼450 nm), an unusually small hyperfine coupling constant in the $g_z$ region of its electron paramagnetic resonance (EPR) spectrum, and a high reduction potential.[3] Besides these similarities with other cupredoxins, UMC shows a number of unusual features which have attracted attention, including (i) an axial Gln ligand (a feature of the stellacyanins) in place of the typical Met (all cupredoxins have two His and one Cys ligands) at the type 1 (T1) copper site, (ii) pH-induced changes in the UV−vis spectrum (both LMCT bands shift toward shorter wavelength) upon increasing pH[1] (an alkaline transition), and (iii) the unknown physiological function (for all phytocyanins) which is probably related to ET. These considerations make phytocyanins a prominent target for spectroscopic investigation, and hence, effort has been devoted to understanding UMC using an array of experimental techniques.[4,5] Resonance Raman (RR) measurements of UMC have recently yielded information on the vibrational dynamics that improve the description of Cu(II) site and its environment.[6] However, this method cannot give a complete picture of certain processes, such as the nature of nuclear dynamics in excited states and the coupling among the protein's electronic levels. This information is needed, because lower-energy excited states serve as acceptor levels when the protein receives an electron from a redox partner. Time-domain vibrational spectroscopy gives information that is complementary (but not identical) to that obtained from frequency-domain Raman. In particular, femtosecond pump−probe spectroscopic studies on the paradigmatic blue copper proteins azurin and plastocyanin[7−11] have demonstrated that this technique enables real-time analysis, in addition to excited-state population dynamics, of vibrational motions coupled to electronic transitions. In fact, if the system is excited in the LMCT band by a very short pulse (that is, a pulse with a duration shorter than the periods of the vibrations coupled to the transition), vibrational coherence is induced in both the ground and excited electronic states. Impulsive coherent vibrational spectroscopy is a powerful complement to RR with some particular strengths: (i) It provides information on the vibrational modes coupled to the excited electronic state, which are not accessed by standard RR; (ii) it enables direct time domain probing of low-frequency vibrational modes coupled to the electronic transition, because it circumvents the experimental difficulty of RR in discriminating them from the laser line. For blue copper proteins, excitation in the LMCT band induces a light-driven ET event; hence, the dynamics following the optical preparation of the LMCT band may provide useful information on the processes associated with ET, even if the charge transfer that occurs is not precisely equivalent to the physiological reaction.

* Corresponding author. E-mail address: cannistr@unitus.it.
[†] Università della Tuscia.
[‡] Politecnico di Milano.
[§] University of Newcastle upon Tyne.

10.1021/jp062904y CCC: $33.50 
Published on Web 08/05/2006 PAGE EST: 7.5

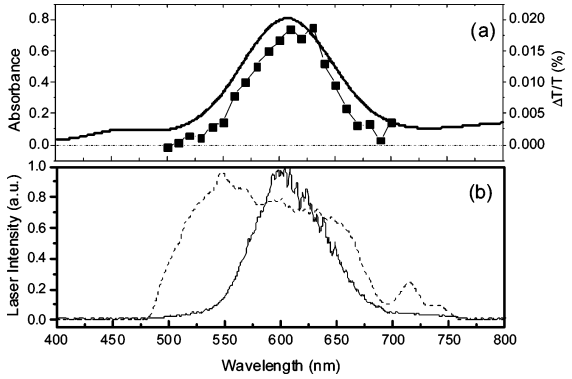


**Figure 1.** (a) Visible absorption spectrum of UMC (solid line) in which the band at 606 nm is the S(Cys) → Cu(II) LMCT transition (see text) and the measured $\Delta T/T$ spectrum of UMC at a fixed delay of 200 fs (■). (b) Pump−pulse (solid line) and probe−pulse (dashed line) spectra of UMC.

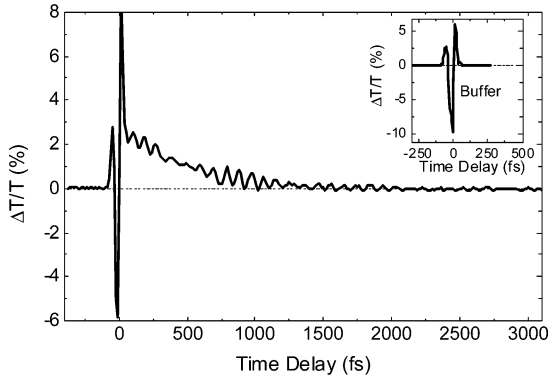


**Figure 2.** Pump−probe trace at a probe wavelength of 660 nm with the inset showing the signal from buffer alone.

However, similar behavior can be assumed,[8] and thus, the investigation of the dynamics of the modes associated with the light-driven reaction gives direct insight into the ET reactivity and possible coupling to motions of the protein.

In this paper, we present a detailed investigation of the ultrafast dynamics of wild-type (WT) UMC. With very short (15-fs) pulses, the dynamics of the excited state and a wide-range Raman spectrum, including the low-frequency region and possible contributions of the excited state, are investigated. Following excitation resonant with the LMCT transition at various probe wavelengths, we observe a main ground-state recovery process with a time constant depending on the investigated spectral component of the transmission difference signal. In particular, the maximum decay time, about 700 fs, is found for the 620-nm spectral component and is significantly longer than for other blue copper proteins. We find evidence of a hot ground-state absorption persisting for several picoseconds. Analysis of the oscillatory pattern superimposed on the signal reveals almost all the vibrational frequencies observed in the conventional RR studies of this protein in addition to a quickly damped mode, assigned to the excited state, and low-frequency modes which could have some biological relevance.

## 2. Experimental Methods

**Sample Preparation and Characterization.** UMC was expressed, isolated, and purified as described previously.[12] For all measurements, UMC was exchanged into 20 mM Tris pH 7.6. Absorption measurements were performed at room temperature using a two-beam UV−vis spectrophotometer (Jasco V-550) in the spectral region 200−800 nm with a 2.0 nm bandpass using a protein concentration of 200 $\mu$M. An absorption spectrum of UMC is shown in Figure 1a.

**Femtosecond Pump−Probe Experiments.** The experimental setup used for the femtosecond pump−probe experiments has been described in detail elsewhere.[13] A mode-locked Ti:sapphire system with chirped pulse amplification produces 500-$\mu$J, 150-fs pulses at a wavelength of 790 nm with a 1-kHz repetition rate. These pulses are used to pump two noncollinear optical parametric amplifiers (NOPAs), which have the capability of generating broadband visible pulses. The first NOPA produces 15-fs transform-limited pulses with a tunable center frequency; the second NOPA generates ultrabroadband visible pulses spanning the 500−700 nm wavelength range (Figure 1b) and a sub-10-fs duration. For both NOPAs, the pulses are compressed by multiple reflections onto chirped dielectric mirrors, which are particularly insensitive to alignment and allow consistently short pulses to be obtained.[14] The pulses derived from the NOPAs are synchronized by a delay line and focused on the sample using reflective optics, in a standard noncollinear pump−probe configuration; an intense pulse from the first NOPA serves as the pump, while a weaker, delayed pulse from the second NOPA probes the differential transmission changes ($\Delta T/T$). For our experiments, the pump pulse was tuned to 610 nm (Figure 1b), to achieve optimum overlap with the UMC absorption, and pump and probe beams were set to parallel polarization. After passing through the sample, the probe beam is spatially selected by means of an iris and sent to a slow detector. Time-resolved measurements at specific probe wavelengths (spectral components of the signal) were obtained by spectral filtering, with 10-nm bandwidth interference filters, the probe beam after it passed through the sample and combining differential detection with lock-in amplification. Transmission difference spectra over the entire bandwidth of the probe pulse, at specific delays, are then reconstructed from the time traces, after low-pass filtering, in order to suppress the coherent oscillations superimposed on the dynamics. By inserting a mirror before the sample, it is possible to perform a noncollinear cross-correlation between pump and probe pulses in a 100-$\mu$m-thick $\beta$-barium borate crystal, so as to exactly determine the zero time delay and the instrumental response function. Day-to-day measurements yielded consistently a width of 15−20 fs for the cross-correlation.

The solutions were kept at room temperature in a homemade cuvette, employing 200-$\mu$m-thick fused silica windows and with an optical path of ∼400 $\mu$m. Experiments typically required 50 $\mu$L of sample at a concentration of 0.86 mM. Since the average power is quite low, in the microwatt range, no sample degradation was observed; nevertheless, the solution was replaced at the beginning of each experimental run. Excitation intensity was maintained in the linear regime, with $\Delta T/T$ below 5−6%. Absorption spectra of UMC were taken immediately before and immediately after the pump−probe measurements to check for photodegradation.

## 3. Results and Analysis

Figure 2 shows a typical $\Delta T/T$ trace for UMC following excitation with a 15-fs pulse at 610 nm. We observe an increased transmission ($\Delta T/T > 0$), which should be due to photobleaching (PB) of the ground state of the LMCT transition and to a stimulated emission (SE) from the excited state (if a SE process occurs in UMC, it can only be detected by pump−probe measurements, because UMC, like other cupredoxins, has no fluorescence emission in the investigated region). The $\Delta T/T$

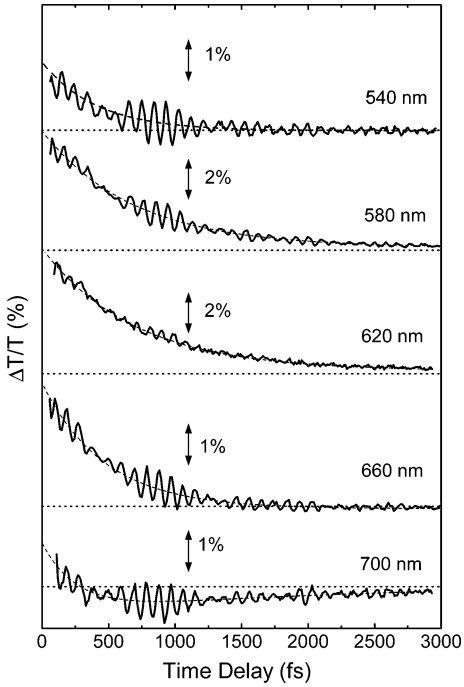


**Figure 3.** Measured $\Delta T/T$ (solid lines) of UMC as a function of pump−probe delay, at different probe wavelengths, with exponential fits shown as dashed lines. The horizontal lines indicate the zero level for each curve.

signal decays on the picosecond time scale, indicating fast recovery of the ground-state population. Superimposed on this decay is an oscillatory pattern, assigned to vibrational coherence, created by the very short pump pulses in the excited and ground states multidimensional potential energy surfaces (PESs).[15] The signal possesses an artifact around zero time delay that is due to the nonresonant response by the buffer solution. This artifact, however, should vanish when the response of the buffer solution ceases, which will happen when pump and probe are well-separated temporally. The inset of Figure 2 demonstrates that the signal from the buffer solution becomes negligible at around 60 fs, and at greater time delays we therefore detect the pure protein signal. Figure 3 shows a series of $\Delta T/T$ traces at different probe wavelengths, starting from 60 fs. The same qualitative behavior seen in Figure 2 is observed at all available probe wavelengths in the 500−700 nm range. Various theoretical models have been used to describe the decay process which dominates these experimental data. For all traces but one, the best description of the differential transmission decay was based on the hypothesis of a single decaying exponential plus a constant offset [$y(t) = a_1 \cdot \exp(-t/\tau_1) + y_0$]. For the signal detected at 700 nm, a fit to this model left an exponential residual, and thus, in agreement with previous studies,[7] a second exponential was added to the fitting function [becoming $y(t) = a_1 \cdot \exp(-t/\tau_1) + a_2 \cdot \exp(-t/\tau_2) + y_0$]. The fitting curves are shown in Figure 3 and the corresponding parameters in Table 1.

A quantitative analysis of the traces highlights some remarkable differences. (i) The decay time constants are wavelength-dependent, ranging from 270 to 700 fs. The longest time constant is observed for the signal detected at 620 nm, while shorter time constants are observed at both longer and shorter probe wavelengths. Notably, the 620-nm spectral component is close to the peak of the ground-state absorption, which has a maximum at around 600 nm (the $\Delta T/T$ spectrum, reported in Figure 1a, also shows a maximum at around 600 nm). (ii) At a

**TABLE 1: Parameters for the Exponential Fits to the Pump−Probe Signals Shown in Figure 3**

| $\lambda$ (nm) | $a_1$ (%) | $\tau_1$ (fs) | $a_2$ (%) | $\tau_2$ (fs) | offset (%) |
|---|---|---|---|---|---|
| 540 | 1.64 | 409 | | | −0.014 |
| 580 | 5.74 | 686 | | | 0.13 |
| 620 | 6.04 | 693 | | | 0.14 |
| 660 | 3 | 471 | | | −0.057 |
| 700 | 1.71 | 274 | −0.74 | 1840 | 0.1393 |

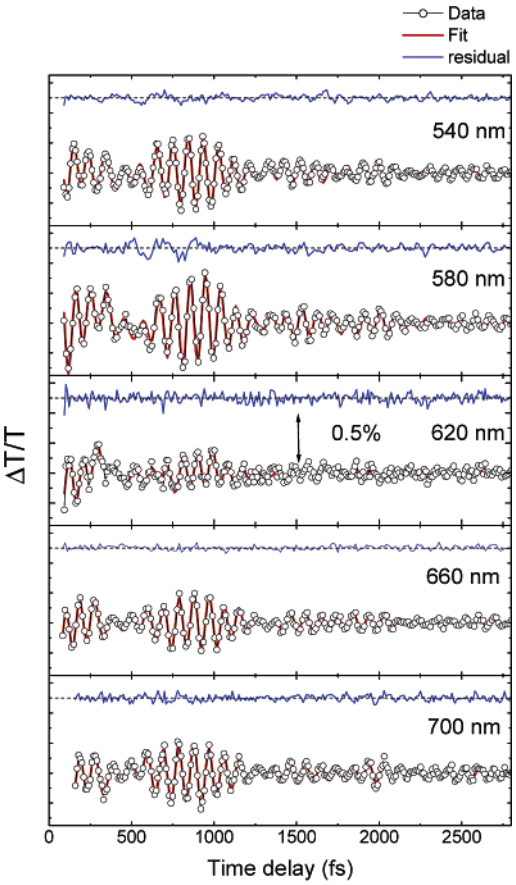


**Figure 4.** Oscillatory component of the signals following subtraction of an exponential decay (circles) along with fits by a sum of damped cosinusoids (solid lines). The upper trace in each panel is the residual after interpolation.

probe wavelength of 700 nm, the positive $\Delta T/T$ signal decays rapidly ($\tau_1 = 270$ fs) and gives rise to a negative signal, indicating a photoinduced absorption (PA); this PA signal in turn decays back to the baseline with a longer time constant ($\tau_2 \approx 2$ ps).

The oscillatory components of the $\Delta T/T$ signal, after subtraction of the population decay, are reported in Figure 4 as circles. These oscillations also display a wavelength dependence, both in amplitude and in phase. The Fourier transform amplitudes of the oscillatory components of the signal at different probe wavelengths are shown in Figure 5. The 10-fs step of the pump−probe traces allows detection, according to the sampling theorem, of oscillations with frequencies up to 1666 $cm^{-1}$, much higher than those analyzed in this paper. Additionally, the 2800-fs observation time limits the minimum observable full width at half-maximum line width to ∼14 $cm^{-1}$. Three major peaks, at 346, 382, and 408 $cm^{-1}$ (the first having the highest intensity at all probe wavelengths), are present in all spectra along with features around 230 $cm^{-1}$. In addition, a peak around 50 $cm^{-1}$ is clearly evident in the spectra corresponding to probe

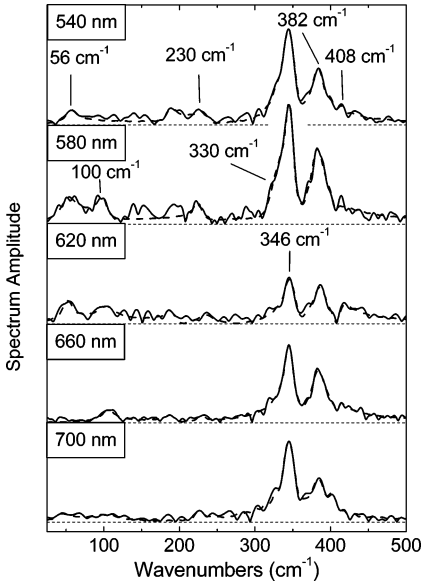


**Figure 5.** Fourier transform amplitudes of the oscillatory components of the exponential decays (solid lines) and of the fits (dotted lines) of these data to the sum of damped cosinusoids, $s(t)$.

wavelengths of 540, 580, and 620 nm, while a peak around 100 $cm^{-1}$ is prominent at probe wavelengths of 580, 620, and 660 nm.

To obtain information about coherent vibrational dynamics (damping time and phase) of single modes, the oscillatory component was modeled by a sum of damped cosinusoids

$$s(t) = \sum_{i=1}^{n} A_i \exp(-t/\tau_i) \cos(\omega_i t + \phi_i)$$

We used a nonlinear fitting procedure in which frequencies $\omega_i$, phases $\phi_i$, amplitudes $A_i$, and damping times $\tau_i$ were adjusted iteratively in order to minimize the root-mean-square error between experiment and model. Only components with absolute amplitudes ($A_i$) higher than 0.001 have been retained. The starting frequencies for the fit were obtained from the Fourier transforms of the oscillatory components. The fitting curves are shown in Figure 4 as solid lines, and the corresponding Fourier transforms are reported in Figure 5 as dashed lines. In Tables 2 and 3, the fitting parameters obtained for high and low frequencies, respectively, are summarized. Regarding the high-frequency components, the position and damping times of the main peaks are constant (except for the 330-$cm^{-1}$ line). This is not the case for the low-frequency modes, which have highly variable properties over the investigated spectral range. The results have been confirmed by a linear prediction single value decomposition analysis (not shown).[16]

## 4. Discussion

**Population Dynamics.** Our results, indicating a fast ground-state recovery following excitation of the LMCT transition in UMC, can be compared to those of previous pump−probe studies on similar proteins, taking into account the energy level scheme describing the LMCT bands of a T1 copper site[17−20] (Figure 6 and Table 4). Edington et al.[7] excited spinach plastocyanin into its LMCT band (620 nm) with 80-fs pulses and detected the signal at 625 nm. They inferred a two-step relaxation process for the excited state by a hole transfer process, first into an intermediate excited d state with a 125-fs lifetime, and from this to the ground state with a 285-fs time constant. This two-step relaxation process, in terms of a hole transfer representation, can be described as

$$\text{S(Cys-}\pi) \xrightarrow{125\text{ fs}} \text{Cu } d_{xz+yz} \xrightarrow{280\text{ fs}} \text{Cu } d_{x^2-y^2}$$

Other studies have found single decay processes for the excited states of blue copper proteins. Nakashima et al.[9] observed a 270-fs decay time for the ground-state recovery in plastocyanin from *Synechococcus* PCC7942 when excited with a 33-fs pulse at 635 nm. Cimei et al. have investigated azurin[10] and poplar plastocyanin[11] by exciting the sample with a 10-fs pulse centered at 550 nm and analyzing the differential transmission at 580 and 560 nm. In both cases, it was found that the temporal differential transmission can be fit by a single exponential with a time constant around 270 fs and an offset of ∼3%. Book et al.[8] reported pump−probe measurements, for poplar and spinach plastocyanins and human ceruloplasmin, by exciting with 16-fs pulses centered at 770 nm and investigating both the integrated and spectrally resolved (750- and 800-nm spectral components) probe signals. A decaying exponential with a time constant of about 280 fs and an offset of about 2% was found (these were similar for integrated and wavelength resolved differential transmission). However, at variance with the other studies, the excitation wavelength in this study (770 nm) corresponds to a weak absorption band due to a combination of three Cu d−d transitions. Thus, this study addressed only the second step of the de-excitation process postulated by Edington et al.

In all the above studies, fast ground-state recovery indicates strong nonradiative coupling between the ground and excited electronic states. This ultrafast internal conversion (IC) process can be interpreted as a metal-to-ligand charge-transfer (MLCT) process. Almost all the previously described pump−probe studies on blue copper protein dynamics after excitation of the main LMCT transition have used a single spectral component or at maximum two spectral components of the transmitted signal, usually corresponding to probe wavelengths very near to the pump. In fact, a spectral component analysis was reported by Book et al.,[8] who investigated only the d−d transitions. Thus, a direct comparison with the literature can be made for the spectral components near the excitation wavelength in UMC (that is, the 580- and 620-nm spectral components which correspond to the LMCT absorption). For UMC, both these spectral components show a single-step deactivation process with a time constant of ∼700 fs, in terms of a hole transfer representation

$$\text{S(Cys-}\pi) \xrightarrow{700\text{fs}} \text{Cu } d_{x^2-y^2}$$

indicating a lower excited-state deactivation rate with respect to the previously studied proteins. This could indicate altered coupling between the Cu−S and the d−d transitions in UMC with respect to the other proteins investigated. UMC has a different T1 copper site structure compared to the other blue copper proteins studied by pump−probe spectroscopy with an axial Gln ligand instead of the more customary (and weaker) Met.[21] The enhanced axial interaction in UMC leads to a decreased equatorial ligand field strength and Cu−S interaction with respect to plastocyanin and azurin.[21] Transition energies are reported in Table 4 for spinach plastocyanin and *Cucumis sativus* stellacyanin (CST), a protein very similar to UMC. The data show a larger energy gap between Cys and Cu(d−d) transitions in the stellacyanin, which has been shown to be

**TABLE 2: Parameters for the Damped Cosinusoid Fits to the High-Frequency Oscillatory Components of the Pump−Probe Signals Shown in Figure 4**

| $\omega$ | ~330 cm$^{-1}$ [a] | | | 346 cm$^{-1}$ | | | 382 cm$^{-1}$ | | | 408 cm$^{-1}$ | | |
|---|---|---|---|---|---|---|---|---|---|---|---|---|
| $\lambda$ (nm) | $A_1$ (%) | $\tau_1$ (fs) | $\phi_1$ (rad) | $A_2$ (%) | $\tau_2$ (fs) | $\phi_2$ (rad) | $A_3$ (%) | $\tau_3$ (fs) | $\phi_3$ (rad) | $A_4$ (%) | $\tau_4$ (fs) | $\phi_4$ (rad) |
| 540 | 0.886 | 268 | −0.81 | 0.807 | 857 | 1.63 | 0.609 | 656 | 2.0 | 0.146 | 1401 | 3.15 |
| 580 | 0.456 | 480 | −1.53 | 0.66 | 1135 | 0.8 | 0.818 | 625 | 1.15 | 0.228 | 1013 | 2.57 |
| 620 | 1.147 | 140 | 1.42 | 0.358 | 907 | −2.18 | 0.444 | 596 | −2.67 | 0.179 | 721 | −2.40 |
| 660 | 2.410 | 91 | −2.94 | 0.511 | 1006 | −0.55 | 0.656 | 614 | −0.57 | 0.136 | 1308 | 0.15 |
| 700 | 3.760 | 77 | −1.22 | 0.548 | 1033 | −0.44 | 0.576 | 629 | −0.22 | 0.092 | 2306 | 0.80 |

[a] Given the fast dephasing of the 330-cm$^{-1}$ mode, there is some uncertainty as to the exact frequency of this mode, which actually ranges from 300 to 340 cm$^{-1}$.

**TABLE 3: Parameters for the Damped Cosinusoid Fits to the Low-Frequency Oscillatory Components of the Pump−Probe Signal Shown in Figure 4**

| $\lambda$ (nm) | $\omega_1$ (cm$^{-1}$) | $A_1$ (%) | $\tau_1$ (fs) | $\phi_1$ (rad) | $\omega_2$ (cm$^{-1}$) | $A_2$ (%) | $\tau_2$ (fs) | $\phi_2$ (rad) | $\omega_3$ (cm$^{-1}$) | $A_3$ (%) | $\tau_3$ (fs) | $\phi_3$ (rad) |
|---|---|---|---|---|---|---|---|---|---|---|---|---|
| 540 | ***56*** | 0.0045 | 819 | −2.06 | | | | | ***232*** | 0.0046 | 769 | −2.89 |
| 580 | ***52*** | 0.0111 | 577 | −2.66 | ***99*** | 0.0052 | 991 | 0.36 | ***225*** | 0.0037 | 1157 | −2.12 |
| 620 | ***51*** | 0.0052 | 1040 | −2.94 | ***103*** | 0.0087 | 467 | 0.3 | ***235*** | 0.0037 | 641 | 1.07 |
| 660 | ***44*** | 0.0041 | 713 | 1.51 | ***106*** | 0.0038 | 836 | 1.28 | ***228*** | 0.0015 | 1467 | 1.35 |
| 700 | ***66*** | 0.0056 | 512 | −1.16 | ***105*** | 0.0092 | 329 | 2.03 | ***226*** | 0.0020 | 1358 | 1.15 |

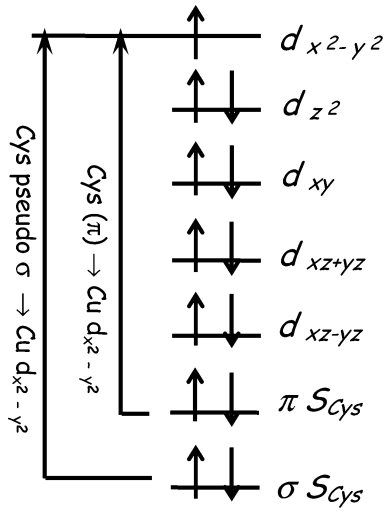


**Figure 6.** Relative energy of the atomic orbitals in blue copper proteins. The ground-state configuration of the copper d orbital and the S(Cys) orbitals involved in the visible transitions are shown. The energy level spacings are not drawn to scale (see Table 4).

**TABLE 4: Transition Energies with Respect to the Cu $d_{x^2-y^2}$ Level for *Cucumis sativus* Stellacyanin (CST) and Spinach Plastocyanin (sPC)**

| | energy (cm$^{-1}$) | |
|---|---|---|
| band | CST[a] | sPC[b] |
| Cu $d_{z^2}$ | 5500 | 5000 |
| Cu $d_{xy}$ | 8800 | 10800 |
| Cu $d_{xz+yz}$ | 11200 | 12800 |
| Cu $d_{xz-yz}$ | 12800 | 13950 |
| Cys $\pi$ | 16800 | 16700 |
| Cys pseudo $\sigma$ | 18600 | 18700 |

[a] Data for taken from ref 19. [b] Data for sPC taken from ref 20.

related to the strength of the axial ligand.[19] In UMC, the ligand-field bands are probably at even lower energy than in CST, since the corresponding absorption bands are centered at around 860 nm as compared to ~830 nm in CST.[19,22,23] From the present study, it seems that this increased energy gap disfavors a two-step MLCT process inducing direct deactivation of the first half-occupied Cu level to the ground state, which is therefore less efficient than the processes occurring in the other cupredoxins studied. It is also possible that coupling among Cu and Cys levels is lower in UMC. If the hypothesis holds that the MLCT transition can be considered analogous to the physiological reaction, the slower deactivation rate of this transition in UMC indicates less efficient ET. Interestingly, this interpretation is in agreement with the suggestion that a strong axial Gln ligand diminishes ET reactivity in cupredoxins.[2,21−23] In fact, the electron self-exchange (ESE) rate constant of UMC is lower than in other cupredoxins and becomes comparable to that of plastocyanin, for example, when the Gln ligand is substituted by the more usual Met.[22,24] In addition, donor−acceptor electronic coupling is probably enhanced for T1 copper sites with weaker axial ligands.[19]

Another key feature of the excited-state decay times of UMC is their significant probe wavelength dependence; the longest recovery time is observed around the peak of the absorption band (620 nm), while shorter times are found at higher and lower wavelengths (see Table 1). Several explanations for this wavelength dependence of the ground-state recovery can be given. First, it is worth recalling that the main LMCT band (around 600 nm) of cupredoxins (including the stellacyanins), in which both pump and probe pulses fall, is the superposition of the main S(Cys-$\pi$) → Cu $d_{x^2-y^2}$ band and a weaker S(Cys-pseudo $\sigma$) → Cu $d_{x^2-y^2}$ LMCT transition (see Figure 6 and Table 4).[19] The observed $\Delta T/T$ dynamics therefore probably result from the overlap of the different PB/SE processes for each of these LMCT transitions, which have their own dynamics. The product should be wavelength-dependent, because the relative contribution to the signal of each band changes with the probe wavelength. Another possible reason for the wavelength-dependent lifetimes is the occurrence of vibrational relaxation within the excited state. It must be recalled that the positive $\Delta T/T$ signal may result from a superposition of ground-state PB and SE from the excited state. The pump pulse, according to the Franck−Condon (FC) principle, generates an excited-state wave packet with an excess vibrational energy, which is then lost by intramolecular vibrational relaxation (IVR), typically on the 100-fs time scale, as the wave packet relaxes to the bottom of the excited-state well;[25,26] IVR therefore causes a red shift of the SE spectrum. An alternative explanation for the red shift of the SE could be ultrafast solvation, i.e., reorganization of the protein environment around the chromophore so as to lower the energy of the excited state.[26] Notably, environment

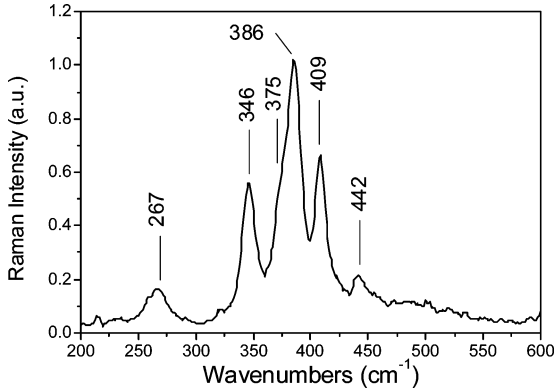


**Figure 7.** Resonance Raman spectrum of Cu(II) UMC obtained by exciting with 633-nm laser radiation. Measurements were carried out on a 0.86 mM UMC solution at pH 7.0.[6]

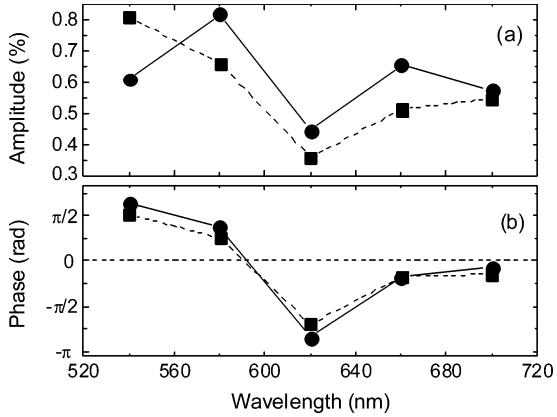


**Figure 8.** Probe wavelength dependence of amplitude (a) and phase (b) of the main [346 $cm^{-1}$ (■) and 382 $cm^{-1}$ (●)] oscillating components of the pump−probe traces.

reorganization effects should be greater in UMC than in plastocyanin and azurin, because its active site is more solvent-exposed.[2] Both of these effects give rise to a faster decay of the SE signal for short wavelengths with respect to long ones, resulting in an effective wavelength-dependent excited-state lifetime.

At 700 nm, we observe the rapid formation of a weak PA signal, which then decays on the picosecond time scale. This could be due to a small fraction of the excited-state population undergoing a transition to another excited state, from which this PA originates. More likely, however, this can be attributed to absorption by hot ground-state molecules that are formed by the IC process. In a nonradiative electronic transition, the energy of the excited molecule is not emitted in the form of a photon but remains localized on the molecule and its immediate environment. Therefore, the molecule is left in a nonequilibrium ground state, with excess vibrational energy, which results in a pronounced red shift of the ground-state absorption spectrum.[27] Hot ground-state absorption, previously observed in molecules for which the IC process is more rapid than ground-state vibrational relaxation,[28] results in a PA signal to lower energy of the ground-state absorption band. In our case, we observe a decay of the PA with a time constant $\tau = 2$ ps, typical of vibrational relaxation in the ground state.[29]

**Coherent Vibrational Dynamics.** In a pump−probe experiment, wave packets on both the ground-state and excited-state PESs can be generated and detected.[15] Pump−probe spectroscopy involves a three-field interaction with the sample: two of these with the pump, creating a population, and one with the probe, which then interrogates it. For short pump pulses, two fields in the pump pulse can excite, in phase, several vibrational eigenstates of the excited state, creating a coherent superposition in the form of a population wave packet oscillating on the excited-state PES, leaving and returning to the FC region. Another possibility is that the first field induces a polarization wave packet on the excited-state PES, which then propagates for some time during the pump pulse so that the second pump field brings the wave packet back down to the ground state, displaced from the equilibrium position. In this way, ground-state oscillations are generated by a mechanism known as resonant impulsive stimulated Raman scattering (RISRS).[30] Assignment of the observed coherence to the ground or excited state is critical and is based on a comparison with RR spectra and on amplitude, phase, and damping times of the observed oscillations. Thus, it is interesting to compare the time-domain data with the RR spectrum of UMC, which has been reported recently.[6] Briefly, the RR spectrum, shown in Figure 7, consists of five intense peaks at 267, 346, 386, 409, and 442 $cm^{-1}$ and a shoulder around 375 $cm^{-1}$. The modes centered around 400 $cm^{-1}$ have been assigned to mixing of the Cu−S(Cys) stretching vibration with multiple heavy-atom bending modes involving this ligand and adjacent residues.[31] The peak at 267 $cm^{-1}$ has been assigned to the symmetric Cu−N stretch from the histidine ligands.[32,33] The modes arising from the oscillatory part of the time-dependent signal (Figure 5) have frequencies very similar to the RR data but quite different intensities; in particular, the 346 $cm^{-1}$ mode dominates in the time domain data as compared to the 386 $cm^{-1}$ signal in the RR spectrum. This is in agreement with the previously highlighted differences between RR and RISRS approaches in the detection of vibrational modes coupled to an electronic ground state.[34] From our results, it is possible to estimate that the three modes at 346, 382, and 408 $cm^{-1}$ are most likely due to ground-state coherence, because of (i) their close matching to frequencies in the RR spectrum and (ii) their long damping times (in the picosecond range, see Table 2) that are inconsistent with fast excited-state population decay which is expected to destroy excited-state coherence.[35,36] To confirm our assignment, we have studied the probe wavelength dependence of the amplitude and phase of the oscillations, which are plotted in Figure 8 for the two main bands at 346 and 382 $cm^{-1}$. The amplitude of the modulation has a minimum close to the ground-state absorption maximum, while the phase shows a 180° jump around the absorption maximum. These features are consistent with a wave packet oscillating on the ground-state PES.[37,38] The RISRS process, in fact, brings the wave packet back to the ground state with no displacement from its initial position but with added momentum; therefore, a minimum of oscillation amplitude should occur at the absorption peak, while a $\pi$ phase shift is expected between oscillations to the red and to the blue of the absorption maximum.[37,38]

Table 2 shows that, in addition to the three bands mentioned above (at 346, 382, and 408 $cm^{-1}$) which are clearly seen in the Fourier spectra, a fourth mode is observed, with a frequency of ∼330 $cm^{-1}$ and fast damping times, ranging from 80 to 270 fs (given the fast dephasing, there is some uncertainty as to the exact frequency of this mode). In Figure 9, the fitted Fourier spectra obtained with and without this additional mode are compared. We tentatively assign this new rapidly damped mode to an excited-state oscillation. In fact, a strong contribution from the excited-state wave packet is expected, since the duration of the pump pulses (∼15 fs) is significantly shorter than the oscillation periods. On the other hand, the amplitude of this excited-state wave packet should be rapidly damped with time

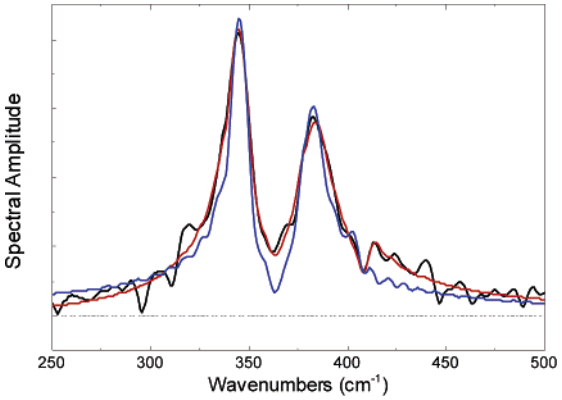


**Figure 9.** Fits of the Fourier spectrum (black line) of the oscillatory component of the pump−probe trace at 660 nm with (red line) and without (blue line) the additional frequency at 330 $cm^{-1}$ with a fast damping time. The fit is improved if the 330 $cm^{-1}$ frequency band is included.

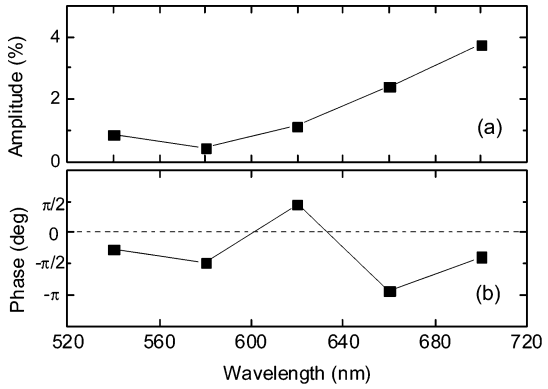


**Figure 10.** Probe wavelength dependence of amplitude (a) and phase (b) of the 330 $cm^{-1}$ oscillating component of the pump−probe traces.

as a consequence of the IC process. The wavelength dependence of amplitude and phase of this new mode are reported in Figure 10; they are markedly different from those of the ground-state modes (see Figure 8). In particular, at variance with RISRS modes, the 330 $cm^{-1}$ mode shows neither a phase shift between oscillations to the red and to the blue of the absorption maximum nor a minimum of the oscillation amplitude at the absorption peak. In addition, the amplitude of the oscillation increases as the probe wavelength increases, suggesting its assignment to the excited state. In fact, for an excited-state mode, one expects a modulation amplitude following the derivative of the emission spectrum, which is red-shifted with respect to the absorption spectrum.[39] Rapidly damped excited-state coherence has already been reported in other systems with short excited-state lifetimes.[40] It appears from Table 2 and Figure 5 that there is no evidence of a 500 $cm^{-1}$ mode, in contrast with the peak found in the pump−probe spectra of spinach[8] and poplar[11] plastocyanin, human ceruloplasmin,[8] and azurin, which is thought to result from Duschinsky rotation.[10] This suggests that no rotation of the ground- and excite-state normal-mode coordinates occurs in UMC. This additional peculiarity of UMC with respect to other cupredoxins further indicates different coupling of ground and excited states in this protein. Interestingly, it has been proposed that Duschinsky rotation can favor ET,[41] and thus, its absence in UMC is in agreement with the above-discussed low efficiency of charge transfer in UMC compared to other cupredoxins.

In the Fourier spectra (see Figure 5 and Table 3), we observe, in addition to the strongly coupled modes discussed above, lower-frequency features, at 56, 101, and 230 $cm^{-1}$. With the exception of the 230 $cm^{-1}$ line, which probably corresponds to the 267 $cm^{-1}$ symmetric Cu−N His mode, these peaks have no counterparts in the RR spectrum of UMC, in agreement with the previously discussed advantage of time-domain vibrational spectroscopy in detecting low-frequency modes.[42] Similar low-frequency oscillations were reported in the time-domain experiments on other blue copper proteins. In azurin, three vibrational features between 30 and 80 $cm^{-1}$ were observed by both pump−probe[10] and RR[43] studies. Book et al.[8] found low-frequency modes in the 35−55 $cm^{-1}$ region in poplar plastocyanin, spinach plastocyanin, and human ceruloplasmin and assigned these features to protein phonon-like modes coupled to the optical excitation. Nakashima et al.[9] detected low-frequency modes in pump−probe experiments with *Synechococcus* plastocyanin and focused their attention on the strong and quite broad band observed at approximately 30 $cm^{-1}$ that was attributed to a delocalized mode involving motion of the protein skeleton. Cimei et al. found a set of bands in the 22−75 $cm^{-1}$ region in their ultrafast pump−probe study on poplar plastocyanin.[11] Following their interpretation, which is also based on previous inelastic neutron scattering results on blue copper proteins,[44] we attribute the low-frequency bands shown in Figure 5 to collective modes involving large portions of the protein. A number of hypotheses have been suggested to explain the relevance of such collective motions. In general, it is believed that low-frequency collective modes in proteins assist a variety of vital biological processes ranging from ET to catalysis.[45] As an example, it has been shown that collective modes function as a mechanism for an enzyme to achieve substrate specificity.[45] Thus, the evidence of collective modes in UMC during light-driven charge transfer might have some biological relevance, and they could be representative of the molecular rearrangement needed to create an ET pathway.

## 5. Conclusions

In this paper, we have expanded the study of the excited-state dynamics of blue copper proteins by presenting the first pump−probe measurements on a stellacyanin (UMC). Upon excitation with 15-fs pulses resonant with the LMCT transition and detection at several wavelengths, we observe ground-state recovery with wavelength-dependent time constants, from 270 to 700 fs, showing a maximum at the absorption peak of the LMCT band. The longer time constant characterizing the MLCT transition in UMC, with respect to other blue copper proteins, is discussed in connection with parameters describing ET efficiency. Wavelength dependence of the recovery times is explained by (i) the possible excitation of several transitions and (ii) vibrational relaxation within the excited state. Coupled to the population dynamics, we observe vibrational coherence induced by the ultrashort pump pulse. Vibrational activity is mainly seen in the ground state, as expected in a system with fast excited-state decay. However, evidence of a quickly damped oscillation located around 300 $cm^{-1}$ is found, which we assign to the excited state. Finally, we observe low-frequency oscillations which are assigned to collective modes, i.e., modes related to overall protein motions, suggesting participation of the protein matrix in the relaxation process.

## References and Notes

(1) Dennison, C.; Lawler, A. T. *Biochemistry* **2001**, *40*, 3158−3166.
(2) Koch, M.; Velarde, M.; Harrison, M. D.; Echt, S.; Fischer, M.; Messerschmidt, A.; Dennison, C. *J. Am. Chem. Soc.* **2005**, *127*, 158−166.

(3) Dennison, C.; Harrison, M. D. *J. Am. Chem. Soc.* **2004,** *126*, 2481−2489.
(4) Dennison, C.; Harrison, M. D.; Lawler, A. T. *Biochem. J.* **2003** *371*, 377−383.
(5) Nersissian, A. M.; Mehrabian, Z. B.; Nalbandyan, R. M.; Hart, P. J.; Fraczkiewicz, G.; Czernuszewicz, R. S.; Bender, C. J.; Peisach, J.; Herrmann, R. G.; Selverstone Valentine, J. *Protein Sci.* **1996**, *5*, 2184−2192.
(6) Delfino, I.; Sato, K.; Harrison, M. D.; Andolfi, L.; Bizzarri, A. R.; Dennison, C.; Cannistraro, S. *Biochemistry* **2005**, *44*, 16090−16097.
(7) Edington, M. D.; Diffey, W. M.; Doria, W. J.; Riter, R. E.; Beck, W. F. *Chem. Phys. Lett.* **1997**, *275*, 119−126.
(8) Book, L. D.; Arnett, D. C.; Hu, H.; Scherer, N. F. *J. Phys. Chem. A* **1998**, *102*, 4350−4359.
(9) Nakashima, S.; Nagasawa, Y.; Seike, K.; Okada, T.; Sato, M.; Kohzuma, T. *Chem. Phys. Lett.* **2000**, *331*, 396−402.
(10) Cimei, T.; Bizzarri, A. R.; Cannistraro, S.; Cerullo, G.; De Silvestri, S. *Chem. Phys. Lett.* **2002**, *362*, 497−503.
(11) Cimei, T.; Bizzarri, A. R.; Cerullo, G.; De Silvestri, S.; Cannistraro, S. *Biophys. Chem.* **2003**, *106*, 221−231.
(12) Harrison, M. D.; Dennison, C. *Proteins* **2004**, *55*, 426−435.
(13) Manzoni, C.; Polli, D.; Cerullo, G. *Rev. Sci. Instrum.* **2006**, *77*, 023103/1−023103/9.
(14) Zavelani-Rossi, M.; Cerullo, G.; De Silvestri, S.; Gallmann, L.; Matuschek, N.; Steinmeyer, G.; Keller, U.; Angelow, G.; Scheuer, V.; Tschudi, T. *Opt. Lett.* **2001**, *26*, 1155−1157.
(15) Pollard, W. T.; Dexheimer, S. L.; Wang, Q.; Peteanu, L. A.; Shank, C. V.; Mathies, R. A. J. *Phys. Chem.* **1992**, *96*, 6147−6158.
(16) Barkhuijsen, H.; de Beer, R.; Bovee, W. M.; Creyghton, J. H.; van Ormondt, D. *Magn. Reson. Med.* **1985**, *2*, 86−89.
(17) Solomon, E. I.; Hare, J. W.; Dooley, D. M.; Dawson, J. H.; Stephens, P. J.; Gray, H. B. *J. Am. Chem. Soc.* **1980**, *102*, 168−178.
(18) Penfield, K. W.; Gray, R. R.; Himmelwright, R. S.; Eickman, N. C.; Norris, V. A.; Freeman, H. C.; Solomon, E. I. *J. Am. Chem. Soc.* **1981**, *103*, 4382−4388.
(19) DeBeer George, S.; Basumallick, L.; Szilagyi, R. K.; Randall, D. W.; Hill, M. G.; Nersissian, A. M.; Valentine, J. S.; Hedman, B.; Hodgson, K. O.; Solomon, E. I. *J. Am. Chem. Soc.* **2003**, *125*, 11314−11328.
(20) Basumallick, L.; Szilagyi, R. K.; Zhao, Y.; Shapleigh, J. P.; Scholes, C. P.; Solomon, E. I. *J. Am. Chem. Soc.* **2003**, *125*, 14784−14792.
(21) Dennison, C. *Coord. Chem. Rev.* **2005**, *249*, 3025−3054.
(22) Harrison, M. D.; Dennison, C. *ChemBioChem* **2004**, *5*, 1579−1581.
(23) Yanagisawa, S.; Dennison, C. *J. Am. Chem. Soc.* **2005**, *127*, 16453−16459.
(24) Sato, K.; Kohzuma, T.; Dennison, C. *J. Am. Chem. Soc.* **2003**, *125*, 2101−2112.
(25) Stratt, R. M.; Maroncelli, M. *J. Phys. Chem.* **1996**, *100*, 12981−12996.
(26) Jimenez, R.; Fleming, G. R.; Kumar, P. V.; Maroncelli, M. *Nature (London)* **1994**, *369*, 471−473.
(27) Pecourt, J.-M. L.; Peon, J.; Kohler, B. *J. Am. Chem. Soc.* **2001**, *123*, 10370−10378.
(28) Anderson, N. A.; Pullen, S. H.; Walker, L. A.; Shiang, J. J.; Sension, R. J. *J. Phys. Chem. A* **1998**, *102*, 10588−10598.
(29) Lenz, K.; Pfeiffer, M.; Lau, A.; Elsaesser, T. *Chem. Phys. Lett.* **1994**, *229*, 340−346.
(30) Ruhman, S.; Kohler, B.; Joly, A. G.; Nelson, K. A. *Chem. Phys. Lett.* **1987**, *141*, 16−24.
(31) Han, J.; Adman, E. T.; Teruhiko, B.; Codd, R.; Freeman, H. C.; Huq, L.; Loher, T. M.; Sanders-Loher, J. *Biochemistry* **1991**, *30*, 10904−10913.
(32) Loppnow, G. R.; Fraga, E. *J. Am. Chem. Soc.* **1997**, *119*, 896−903.
(33) Qiu, D.; Dong, S.; Ybe, J. A.; Hecht, M. H.; Spiro, T. G. *J. Am. Chem. Soc.* **1995**, *117*, 6443−6446.
(34) Johnson, A. E.; Myers, A. B. *J. Chem. Phys.* **1996**, *104*, 2497−2507.
(35) Dexheimer, S. L.; Wang, Q.; Peteanu, L. A.; Pollard, W. T.; Mathies. R. A.; Shank, C. V. *Chem. Phys. Lett.* **1992**, *188*, 61−66.
(36) Cerullo, G.; Lanzani, G.; Zavelani-Rossi, M.; De Silvestri, S. *Phys. Rev. B* **2001**, *63*, 241104/1−241104/4.
(37) Kumar, A. T. N.; Rosca, F.; Widom, A.; Champion, P. M. *J. Chem. Phys.* **2001**, *114*, 701−724.
(38) Madsen, D.; Stenger, J.; Dreyer, J.; Nibbering, E. T. J.; Hamm, P.; Elsaesser, T. *Chem. Phys. Lett.* **2001**, *341*, 56−62.
(39) Cerullo, G.; Lüer, L.; Manzoni, C.; De Silvestri, S.; Shoshana, O.; Ruhman, S. *J. Phys. Chem. A* **2003**, *107*, 8339−8344.
(40) Lanzani, G.; Zavelani-Rossi, M.; Cerullo, G.; Comoretto, D.; Dellepiane, G. *Phys. Rev. B* **2004**, *69*, 134302/−134302/7.
(41) Sando, G. M.; Spears, K. G.; Hupp, J. T.; Ruhoff, P. T. *J. Phys. Chem. A* **2001**, *105*, 5137−5325.
(42) Zhu, L.; Li, P.; Huang, M.; Sage, J. T.; Champion, P. M. *Phys. Rev. Lett.* **1994**, *72*, 301−304.
(43) Loehr, T. M.; Sanders-Loehr, J. In *Copper Proteins and Copper Enzymes I*; Lontie, R., Ed.; CRC Press: Boca Raton, FL, 1984; p 116.
(44) Bizzarri, A. R.; Paciaroni, A.; Arcangeli, C.; Cannistraro, S. *Eur. Biophys. J.* **2001**, *30*, 443−449.
(45) Zhou, H. X.; Wlodek, S. T.; McCammon, J. A. *Proc. Natl. Acad. Sci. U.S.A.* **1998**, *95*, 9280−9283.